Electronic Supplementary Material (ESI) for Physical Chemistry Chemical Physics.

Electronic Supplementary Information

Strong light-matter interaction in Tungsten Disulfide Nanotubes

Lena Yadgarov[a,b], Bojana Visic[a,c], Tsafrir Abir[b,d], Ron Tenne[e], Alexander Polyakov[f], Roi Levi[a], Tatyana V. Dolgova[g], Varvara V. Zubyuk[g], Andrey A. Fedyanin[g], Eugene A. Goodilin[f], Tal Ellenbogen[d], Reshef Tenne[a] and Dan Oron[e]*

[a.] *Department of Materials and Interfaces, Faculty of Chemistry, Weizmann Institute of Science, Rehovot 76100, Israel.*
[b.] *Department of Condensed Matter Physics, School of Physics and Astronomy, Tel Aviv University, Tel Aviv 69978, Israel.*
[c.] *Condensed Matter Physics Department, Jozef Stefan Institute, Jamova 39, 1000 Ljubljana, Slovenia.*
[d.] *Department of Physical Electronics, School of Electrical Engineering, Tel-Aviv University, Tel Aviv 69978, Israel.*
[e.] *Department of Physics of Complex Systems, Faculty of Physics, Weizmann Institute of Science, Rehovot 76100, Israel*
[f.] *Faculty of Materials Science, Lomonosov Moscow State University, Leninskie Gory 1 -73, 119991 Moscow, Russia*
[g.] *Faculty of Physics, Lomonosov Moscow State University, Leninskie Gory 1 bldg 2, 119991 Moscow, Russia.*
* E-mail: dan.oron@weizmann.ac.il.

Contents

1 Decoupled absorption of dry WS_2 NT calculated from total reflection

In order to separate the scattering and the absorbance processes from the total extinction spectra, decoupled absorption spectrum was measured using an integrating sphere. The method also known as “total reflection” measurement was used to extract the pure absorbance component. The scheme is the following: A dry sample was placed on the pole of the integrating sphere, white a totally scattering standard is placed behind. The incident light was absorbed and reflected/scattered (including all types of scattering by the sample). The reflected/scattered radiation (total reflection) is collected by the integrating sphere and detected by Si photodiode detector. The signal from this detector is subtracted from the incident beam intensity.

1.1 Decoupled scattering signals of the WS_2 NT (ethanol) suspension

The spectra were registered using Perkin Elmer LAMBDA 950 UV/Vis/NIR spectrophotometer equipped with 150 mm Spectralon-coated integrating sphere. A series of geometries were set to characterize different interactions of incident light with WS_2 NT suspension in ethanol. Note that completely the same ethanol suspension of WS_2 nanotubes containing ca. 0.35 mg/ml of WS_2 NT was used in each position. All the spectra were collected in transmission (T, %) coordinates (250-850 nm range, 1 nm step, 0.2 sec signal acquisition duration in each point; 10x10 mm Suprasil^{TM} fused quartz rectangular cuvette was used).

The interaction of the incident light (90^{o} incident angle) with the suspension in the cuvette affords a number of different signals: 1. Directly transmitted; 2. Diffusely transmitted (caused by small-angle, forward and multiple scattering by the particles); 3. Side-scattered (light goes to the side walls of the cuvette); 4. Specularly reflected; 5. Diffusely reflected (caused by backscattering and multiple scattering on the particles); 6. Absorbed (Figure S1a).

In order to find out the impact of the different processes on the light transmission through the WS_2 nanotubes suspension, the cuvette was placed at different positions with respect to the integrating sphere. Some other changes in geometry were made as described below. The following positions were used to identify respective signals:

- Position I (Figure S1b) – direct transmission and small-angle forward scattering
- Position IIa (Figure S1c) – direct transmission and forward scattering
- Position IIb (Figure S1d) – forward scattering
- Position III (Figure S1e) – backscattering
- Position IV (Figure S1f) – total scattering and transmission

The results of these measurements are shown in Figure S1g.

Position I: Common holder for extinction measurements

The cuvette was placed in a common holder for extinction measurements located in 50-60 cm optical distance before the entrance to the integrating sphere. The white Spectralon standard was placed in the reflectance port for this measurement. Directly transmitted light as well as a small part of diffusely transmitted radiation (small-angle forward scattering) were collected by the integrating sphere and were recorded by the detector. Note that in this case, the graph of light transmission through the suspension corresponds to the inverse extinction spectrum.

Position IIa: Transmittance port (directly transmitted beam is included)

The cuvette was placed to the transmission port of the integrating sphere. The white Spectralon standard was placed in the reflectance port for this measurement. In this position, transmission spectrum includes directly and diffusely transmitted (forward scattered) light.

Position IIb: Transmittance port (directly transmitted beam is excluded)

The cuvette was placed to the transmission port of the integrating sphere. The reflectance port was open, so the directly transmitted light was excluded from the transmission spectrum. For this position, transmission spectrum includes just diffusely transmitted light (due to forward scattering).

Position III: Reflectance port (specularly reflected beam is excluded)

The cuvette was placed to the reflectance port, which is mounted at 8^o angle with respect to the incident beam normal plane. No standard sample was placed behind the cuvette mounted to this port. There is a removable part of the integrating sphere wall at the place where specularly reflected beam comes. During the Position III measurement this part of sphere wall was removed and the specularly reflected beam was blocked. Thus, the obtained transmission spectrum corresponds to the diffusely reflected light (mainly due to backscattering).

Position IV: Center of the integrating sphere

The cuvette was suspended in the center of the sphere using a center-mount kit. The white Spectralon standard was placed in the reflectance port for this measurement. In this case, the entire transmitted and (almost) all-angle scattered signals were collected by the integrating sphere and registered by the detector. In this case, the transmission spectrum corresponds to reverse true absorption of the WS_2 nanotubes suspension.

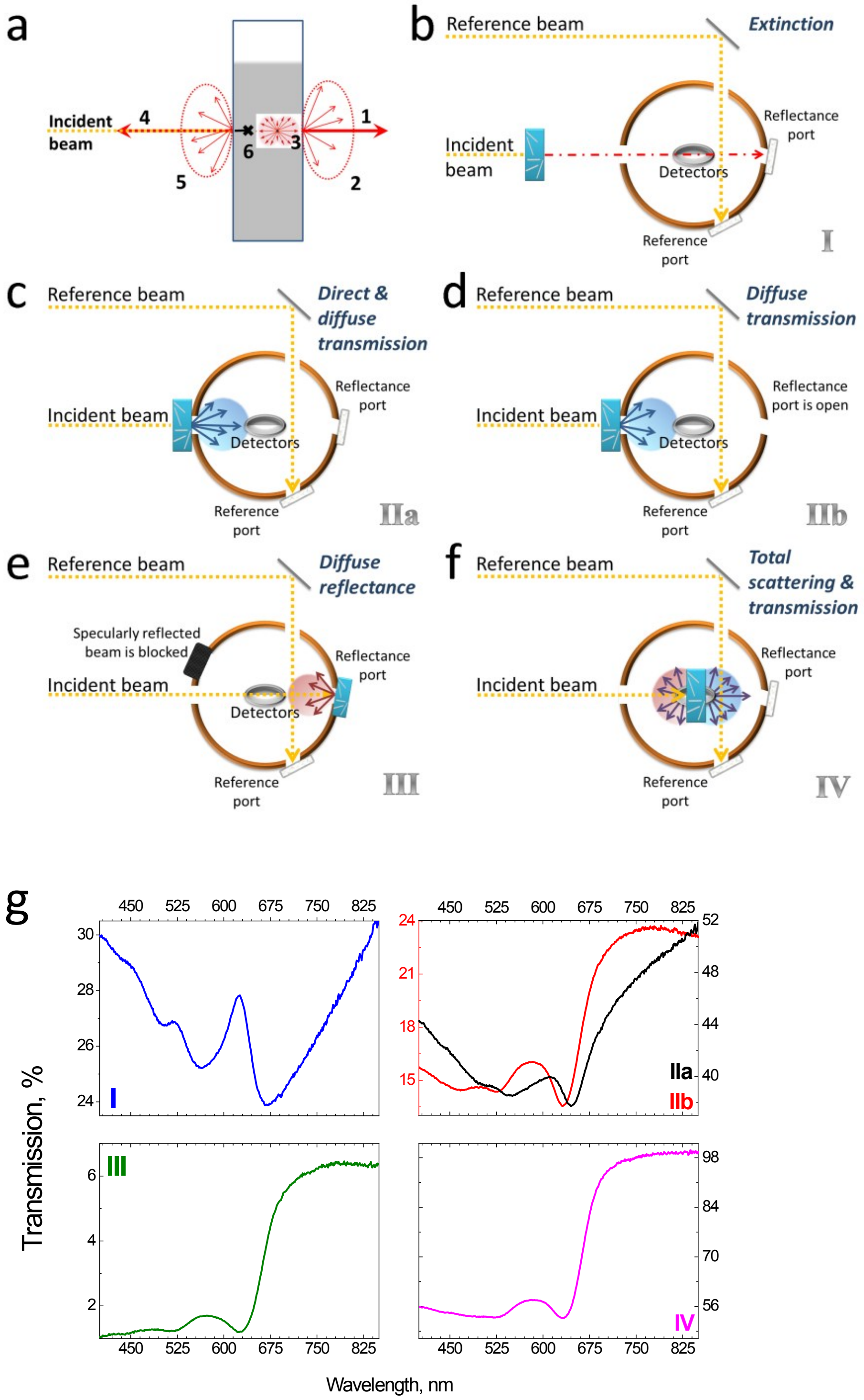

Figure S1. Representation and results of the measurement of different impacts in the light transmission through the WS_2 NT suspension. **(a)** Signals originating from the interaction of light with the suspension**.** Schemes for optical responses of the WS_2 nanotubes suspension in different positions and the integrated sphere geometries: **(b)** common holder for extinction measurements (I); **(c)** transmittance port, directly transmitted beam is included (**IIa**); **(d)** transmittance port, directly transmitted beam is excluded (**IIb**); **(e)** reflectance port, specularly reflected beam is excluded (**III**); **(f)** – suspended center-mount port (**IV**). **(g)** The spectral components of the transmission spectrum: total scattering and transmission (magenta line), direct transmission with forward scattering to the small angles (blue line), forward scattering and direct transmission (black line), forward scattering without direct transmission – diffuse transmission (red line), backscattering – diffuse reflection (olive line).

2 Derivation of the bandgap and the spin-orbit splitting

The spin-orbit splitting between A and B excitons (Δ) was estimated from the difference in the absorbance peak positions of the A and B excitons (Figure 1d, Main text). The direct band gap ($E_{g,dir}$) can be estimated by measuring the Rydberg series of the excited A and B excitons states[1] , see Equation Equation S1 [2].

Equation S1 $E_{g,dir}=E_A+E_{Ryd}$

Where E_A is the A-exciton energy, and E_{Ryd}= 0.042 eV is the exciton Rydberg constant ($E_{An}=E_{An-1}+ E_{Ryd}/n^2$) [3] , where E_{An} is the energy of the n-excited state.

The indirect band gap was calculated as described by Pankove[4] using the absorption measurements (Figure 2, Main text) and Equation Equation S2.

Equation S2
$$\alpha = \frac{A\left(h\nu - E_g\right)^2}{h\nu}$$

Here α is the absorption coefficient, A is a constant and E_g is the indirect band gap of the semiconductor. The results of these calculations are presented in Table 1 - Main text.

3 Coupled oscillator model:

In the phenomenological coupled oscillator (PCO) model, the polarization of a cavity mode and an exciton are described as damped harmonic oscillators coupled through dipole-dipole interaction and forced by an applied electric field. Following Wu et al. [5], the model was extended in order to fit the WS_2 nanotubes, i.e. including both the A and B excitons which couple to a cavity mode. The dynamics of those oscillators is described by Equations **Error! Reference source not found.** to **Error! Reference source not found.**:

Equation S3 $\ddot{x}_{CMR} + \gamma_{CMR}\dot{x}_{CMR} + \omega_{CMR}^2 x_{CMR} - 2\omega_A \cdot g_A x_A - 2\omega_B \cdot g_B x_B = F_{CMR}(t)$

Equation S4 $\ddot{x}_A + \gamma_A \dot{x}_A + \omega_A^2 x_A - 2\omega_A \cdot g_A x_{CMR} = F_A(t)$

Equation S5 $\ddot{x}_B + \gamma_B \dot{x}_B + \omega_B^2 x_B - 2\omega_B \cdot g_B x_{CMR} = F_B(t)$

Where ω_i and γ_i are, respectively, the resonance and damping frequency of the i-th mode ($i = CMR, A, B$ for the cavity mode resonance, A exciton and B exciton, correspondingly). x_i is the time-dependent polarization of the the i-th mode and F_i is the effective force applied by an external field on the i-th mode. g_A (g_B) are the coupling frequencies between the A exciton (B exciton) and the cavity mode.

Since the polarizability of the excitons is expected to be negligible as compared with that of the cavity mode[5] $F_A, F_B \ll F_{CMR}$, and the forces applied on the excitons can therefore be set to 0. The driving force produced by an incident monochromatic wave with frequency ω is presented in Equation **Error! Reference source not found.**:

Equation S6 $F_{CMR}(t) = Re\{F_{CMR}e^{i\omega t}\}$

At steady state, x_{CMR}(t) will follow the driving frequency, as shown in Equation S7:

Equation S7

$$x_{CMR} = Re\left\{\frac{-D_A(\omega)D_B(\omega)}{D_{CMR}(\omega)D_A(\omega)D_B(\omega) - 4\omega_A^2 \cdot g_A^2 D_B(\omega) - 4\omega_B^2 \cdot g_B^2 D_A(\omega)} F_{CMR}e^{i\omega t}\right\}$$

Here we define $D_i(\omega) = \omega_i^2 + i\omega_i\gamma_i - \omega^2$ with the same subscript notation used previously. The work done on the WS_2 nanotubes by the external field, which equals the energy lost by the exciting beam, is calculated as follows:

Equation **S8**

$$C_{ext}\ \alpha\ \langle F_{CMR}\dot{x}_{CMR}\rangle\ \alpha\ \omega Im\left\{\frac{D_A(\omega)D_B(\omega)}{D_{CMR}(\omega)D_A(\omega)D_B(\omega)-4\omega_A^2\cdot g_A^2D_B(\omega)-4\omega_B^2\cdot g_B^2D_A(\omega)}\right\}$$

Here $\langle\cdot\cdot\rangle$ stands for the time average over an oscillation period. The expression in Equation S6 gives us the extinction of an excitation light depending on its frequency ω and can therefore be fitted with the experimental extinction spectra.

Note that attaining a good fit is not a straightforward task as the nanotubes have a rather large diversity in their length and width. However, most WS_2 nanotubes used in these series of experiments have large aspect ratio (>50). The model uses single homogenous oscillators while the real extinction spectrum comprises an ensemble of oscillators which induce broadening of the extinction features. While the scattering spectrum can be fitted quite well using the PCO model, quantitative simulation of the absorption spectrum is far from trivial, as the absorption is dependent upon the rate of radiation emission from the nanotubes and is therefore dependent on the geometric details of the system.

3.1 Estimating the Rabi splitting from the extinction spectrum

In order to calculate the frequencies of the hybridized modes of oscillation one can solve Equation. S3-S5 in the frequency domain. For two oscillators (exciton A and a cavity mode) this task boils down to the solution of the following equation:

Equation S9 $D_A(\omega)\cdot D_{CMR}(\omega)-4\omega_A^2g^2=0$

Here, ω is a complex number whose real part is the frequency of oscillation and its imaginary part is the damping frequency of the mode. In the simplest case of two degenerate oscillators ($\omega_a=\omega_{CMR}$) and negligible damping ($\gamma_A\sim\gamma_{CMR}\sim0$) the frequency splitting between the two modes is given by: **Δω=2g**

This expression for Rabi splitting can be derived by solving the quantum mechanical (QM) Hamiltonian of a three-level system with two degenerate excited states. It therefore shows the equivalence of our model to the QM solution[6].

Next, we examine the more complicated case of non-degenerate lossy oscillator pair. A possible route to graphically solve Equation S9 in this case is to plot the absolute value of the left-hand side of Equation. S9 *versus* the real and imaginary parts of ω· Figure S2a,b shows this method for two coupling conditions: Strong coupling with a low damping rate ($g \gg \gamma_A, \gamma_{CMR}$) and the parameters extracted from the PCO model for the cavity and A exciton alone ($g \sim \gamma_{CMR} \gg \gamma_A$).

In the strong coupling condition, (Figure S2c, top), the maxima of the extinction spectrum overlap with the solutions (zeros) of Equation. S9. Here it's straightforward to extract the Rabi splitting from the extinction spectrum ($320\ meV\ or\ 4.8 \cdot 10^{14}$ Hz). For the parameters of the WS_2 nanotubes (Figure S2c, bottom), however, the situation is quite different. The modes' splitting is smaller than the separation between the extinction peaks due to the high damping rates and the Rabi frequency is estimated as $170\ meV\ (2.6 \cdot 10^{14}$ Hz).

Finally, we graphically find the energies of the resonances for a system consisting of three non-degenerate damped oscillators coupled as in Equation. S3-S5. Here, we find the condition for a non-trivial solution for Equation. S3-S5 without any external forces ($F_A = F_B = F_{CMR} = 0$):

Equation S10 $D_{CMR}(\omega)D_A(\omega)D_B(\omega) - 4\omega_A^2 \cdot g_A^2 D_B(\omega) - 4\omega_B^2 \cdot g_B^2 D_A(\omega) = 0$

Figure SI 2c presents the value of the left-hand side in Equation. S10 vs. the real and imaginary parts of ω. The real values of ω at the minima of the expression (reaching a zero value) are the frequencies of the resonant modes. The corresponding energies of the modes are 2.82 eV, 3.1 eV and 3.74 eV. The measurement data and simulated extinction spectrum appearing on the top show that the modes do not precisely overlap with the extinction. The shift of the extinction peaks is another example for the effect of a relatively high damping rate on the extinction spectrum, similar to the one simulated in Figure SI 2a,b.

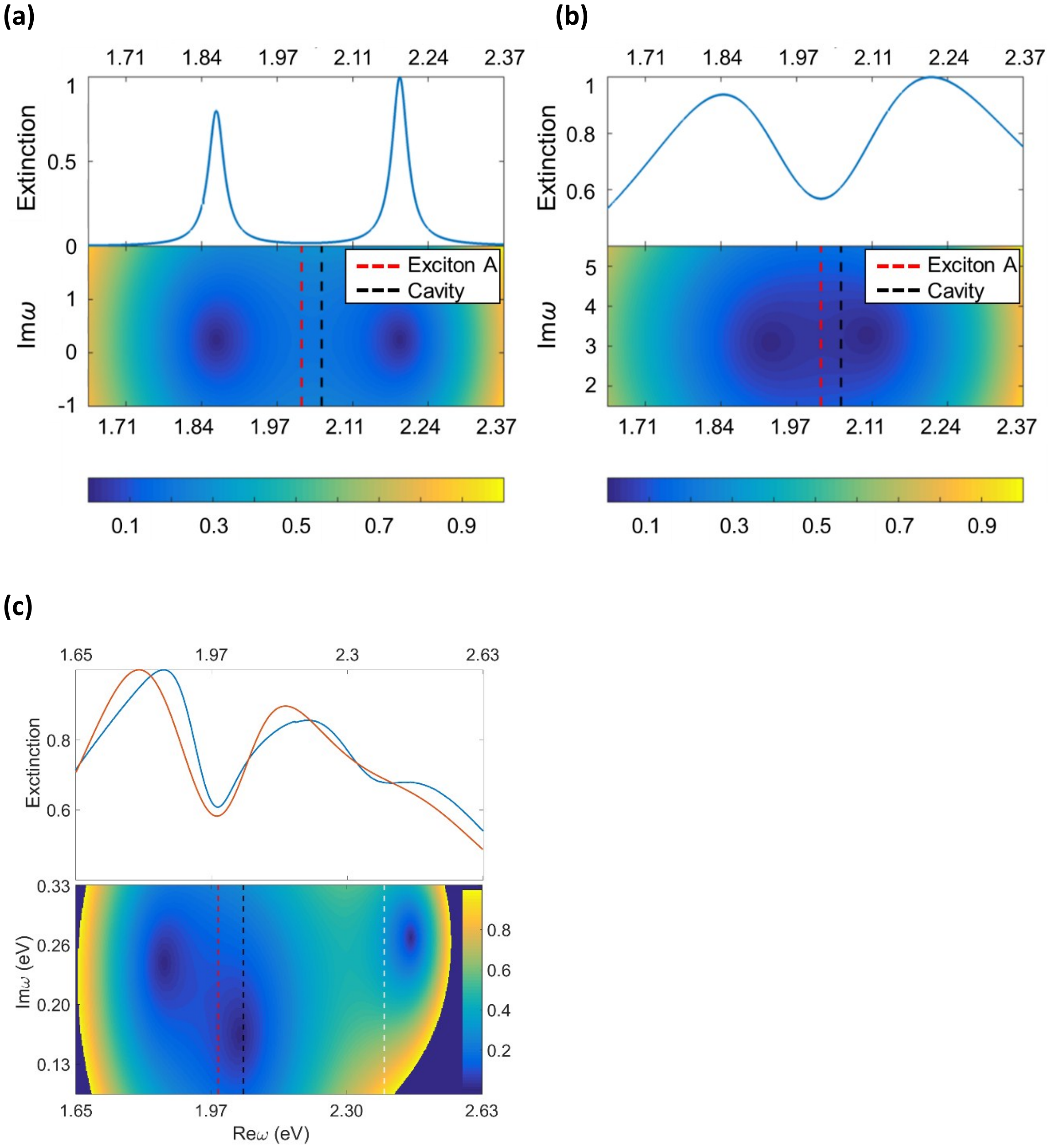

Figure S2. **Graphical solution for the resonant modes' equation for two coupled damped oscillators.** In each panel the calculated extinction spectrum (top) is shown alongside the absolute value of the left-hand side of eq. S9 (SI). In both panels $\lambda_{CMR} = 2.05\ eV(604.5nm), \lambda_A = 2.02\ eV\ (615nm)$ and $g = 0.16\ eV(2.5 \cdot 10^{14}Hz)$ as found from fitting the experimental extinction spectrum. The values of the damping rates for the CMR (exciton) are $5 \cdot 10^{13}Hz$ ($5 \cdot 10^{13}Hz$) in **(a)** and $1.05 \cdot 10^{15}Hz$ ($2.26 \cdot 10^{14}Hz$) in **(b)**; **(c)** Resonant modes in the PCO model for 3 oscillators. (***top***) Experimental data (blue) and PCO fit (red) for the extinction spectrum. (***bottom***) Graphically finding the resonances of the PCO model. The three minima of the expression in the left-hand side of Eq. S10 are the frequencies of the resonant modes of the system. The real values of these correspond to the energies of these states. Black, red, and white dashed lines correspond to position of the CMR, A and B excitons according to the PCO fit.

4 FDTD - finite-difference time-domain simulation

The simulated extinction spectra and TM/TE modes of NW and WS_2 NT is shown in Figure SI 3. As expected, the TM modes of NW and NT are more pronounced (instanced) compared to the TE modes. The transparency dip which appear only in the extinction spectra of WS_2 NT imply that there is a strong interaction between the excitonic features of WS_2 and cavity modes of NW with high refractive index.

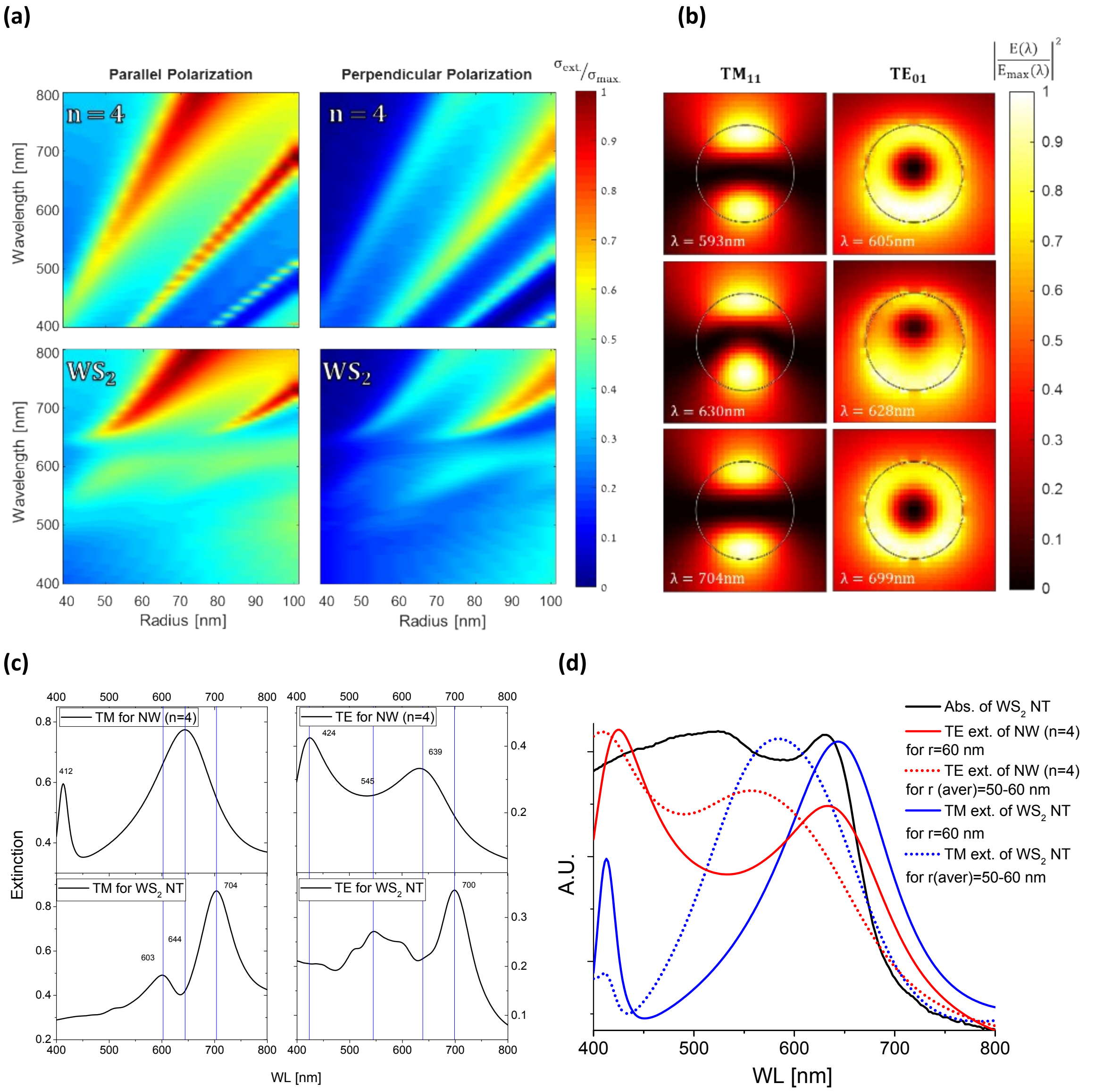

Figure S3. **(a,c)** Extinction spectra of the NW/NT simulated using FDTD method for **(a)** different radii and **(c)** radius of 60 nm; (**up**) constant refractive index (n_{NW}=4) to qualitatively represent WS_2 NT without the effects of the excitons and (**bottom**) with the dielectric data of a bulk WS_2.[7] The irradiation by plane waves polarized parallel (**left**) and perpendicular (**right**) to the nanotube long axis and corresponding to the TM and TE modes, respectively. The blue lines in **(c)** are guide for the eye **(b)** Chosen transverse magnetic/electric (TM/TE) modes for the NW and the WS_2 NT. The values are normalized by the highest value recorded for both polarizations in each set separately. **(d)** Simulated extinction spectra of NW and NT for parallel (TM) and perpendicular (TE) polarizations compared to the measured absorbance of the dispersed NT. That comparison allows to visualize how the excitons overlap with the cavity modes. The dotted lines are the averaged extinction spectra for radius of 50 to 60 nm which better describe the situation in the actual measurement. From this comparison it is obvious that, although the TE (red) modes are weaker, the overlapping between the exciton and the cavity modes is not negligible.

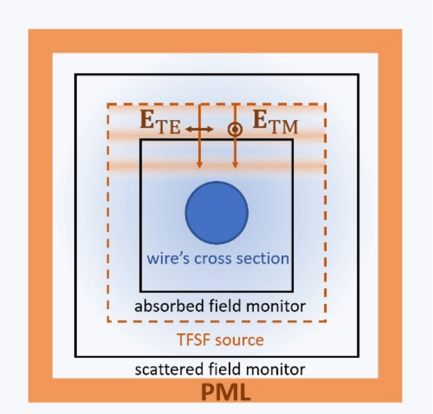

Figure S4. Schematic description of 2D FDTD simulation setup. The cross-section of the nanowires is in the center of the simulation. It is irradiated by a pulse of "total field scattered field" (TFSF) source, which is confined to the orange-dashed square. The polarizations were altered: parallel (TM) and perpendicular (TE) to the wire's long axis. The field monitors record the power absorbed and scattered by the wire. The electric field in the wire's region was recorded as well to get the mode's profiles. Perfectly matched layer (PML) were used as absorbing boundary conditions.

5 Dependence of the extinction of dispersed WS_2 nanotubes on the medium conditions

The position, width and intensity of the scattering peak can be influenced by the solution refractive index (RI) or pH. The UV-vis spectra of the WS_2 nanotubes in different solvents were collected to understand the influence of the RI/pH on the exciton-polariton (EP). In addition, the NP were also measured in solutions with different pHs (1- 14)[i]. The normalized extinction spectra of the nanotubes dispersed in solvents with different RI/pH are shown in (Figure S5a,b). It appears that there is no systematic difference between the extrema positions (Figure S5c,d). Moreover, there is no consistent trend between the pH/RI and the width / intensity / location of the extinction bends.

---

[i] According to the TEM analysis preformed on the NT after the measurement, most of them do not suffer from degradation or surface modification.

As the differences between the nanotube refractive index and that of the surroundings affects the cavity mode resonances (CMRs), it is expected to be shifted as a function of the solution refractive index (RI) or the pH[8] (Table S1). However, the cavity mode of the dispersed WS_2 nanotubes is hybridized with A, B excitons, consequently only the polaritonic modes can be observed in the extinction spectrum. The PCO model fit allows decoupling of the cavity mode band from the excitonic transitions, thus it can be used to observe the shift of the cavity mode band as a function of pH. Indeed, once these extinction spectra were fit using the PCO model, the pH induced shift of the cavity mode became apparent (Figure S5e,f). Notwithstanding this analysis, no clear trend of the uncoupled cavity mode was observed as a function of pH/RI, i.e. the EP shift is random and unpredictable.

Table S1. The RI of the solution were the WS_2 nanotubes were dispersed.

1.027	1.333	1.3498	1.36	1.3616	1.3655	1.372	1.377	1.43	1.431	1.496	1.497
SiO_2 *aerogel*	*Deionized water*	*EtOH/*H_2O *(w/w%) 25/75*	*Ethanol*	*EtOH/*H_2O *(w/w%) 50/50*	*EtOH/*H_2O *(w/w%) 75/25*	*Ethyl acetate*	*Isopropanol*	*Di-methyl-formamide*	*Diethyl glycol*	*Toluene*	*Xylene*

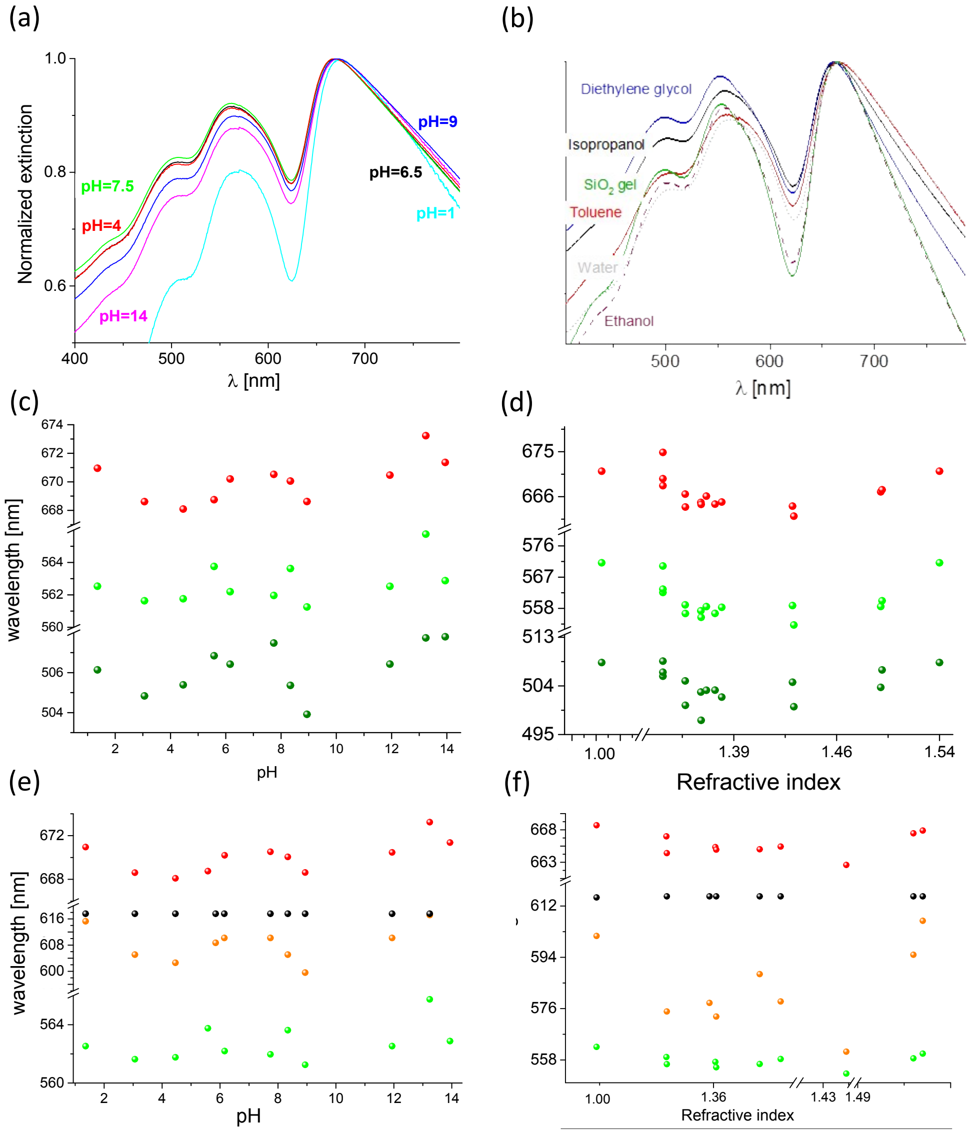

Figure S5. Dependence of the extinction of dispersed WS_2 nanotubes on the medium conditions. (a,b) Extinction spectra of the WS_2 nanotubes dispersed in solutions with various pH **(a)** and refractive indexes **(b); (b,c)** Shift of the maxima peaks as a function of the pH **(c)** and refractive indexes **(d); (e,f)** Extinction maxima (*red and green marks*) of the dispersed WS_2 nanotubes compared to the uncoupled SP (*orange marks*) and exciton A (*black marks*) as a function of the pH **(e)** and refractive indexes **(f)** of that solutions. *RI of the used solvents: SiO_2 aerogel 1.027; deionized water 1.333; Ethanol 1.36; ethyl acetate 1.372; isopropanol 1.377; dimethylformamide 1.43; diethyl glycol 1.431; toluene 1.496; xylene 1.497; mixture: of ethanol and water (w/w%): 25/75 - 1.3498, 50/50 - 1.3616, 75/25 - 1.3655.*

6 Reflectance

For preparation of the WS_2 nanotubes film, the aqueous suspension of the nanotubes was mixed with 1/2 volume of heptane and sonicated in ultrasonic bath for 10 minutes. Within 30 min after sonication, the liquid hydrophobic and aqueous fractions segregated, and a nanotubes film was formed on the liquid-liquid water-heptane interface. The films could be easily transferred onto different substrates like quartz slides and silicon wafers (Figure S6a, b). While the nanotubes in the film are oriented in different angles with respect to each other, they are all confined to the plain of the substrate with no nanotubes protruding outwards. Therefore, in spite of the nanotubes being oriented almost randomly in the plain, the interaction of the *p* and *s*-polarized light remains the same. Therefore, the reflection spectrum of the *s*-polarized light couples strongly to the excitons and exhibits small shift with the incidence angle ϑ. Contrarily, the p-polarized light couples strongly to the excitons in small ϑ and to the cavity mode in large angles of incidence. The extinction spectrum of this film is compared to the absorbance and extinction of the dispersed nanotubes and to the reflectance of the film in Figure S6c. As shown, the EP mode maximum at ~670 nm which appears at the extinction spectrum of the dispersed nanotubes is somewhat diminished and is blue shifted to ~650 nm at the extinction of the film. That phenomenon can be attributed to the morphology of the film. The nanotubes are located only in the plain of the film, such that there are no nanotubes emerging out of the plain. Hence, the scattering intensity is much lower compared to the solvent-dispersed nanotubes.

For the angle/wavelength-dependent reflectivity measurements, an original set-up was used (Figure S7). Halogen lamp (1) was used as a light source. The initial light was collimated using converging lenses (2) while apertures (3) were used to shape a parallel light beam (2 mm in diameter). The Glan prism (4) mounted on a precisely rotating support was used for controlling the linear polarization of the incident light. The WS_2 film nanotubes was deposited on a fused quartz slide and was mounted on a motorized $\vartheta - 2\vartheta$ goniometer (5). The reflected beam was focused to an optical fiber (6) mounted on a swivel mount of a goniometer and connected to Solar S100 spectrometer (7). The reflectivity spectra were collected using *p*-polarized and *s*-polarized incident light at angles ϑ = 5-80° (5° step), 400-1050 nm wavelength range and 1 nm spectral resolution. To normalize the signal intensities of the measured spectra obtained at different ϑ, the same measurements were carried out using 635 nm laser of fixed intensity. Then the spectra sets were normalized using the ratio of reflectivity intensities at given ϑ angle and 635 nm wavelength measured in laser and lamp experiments: $R_{laser}(\vartheta; 635\ nm)/R_{lamp}(\vartheta; 635\ nm)$.

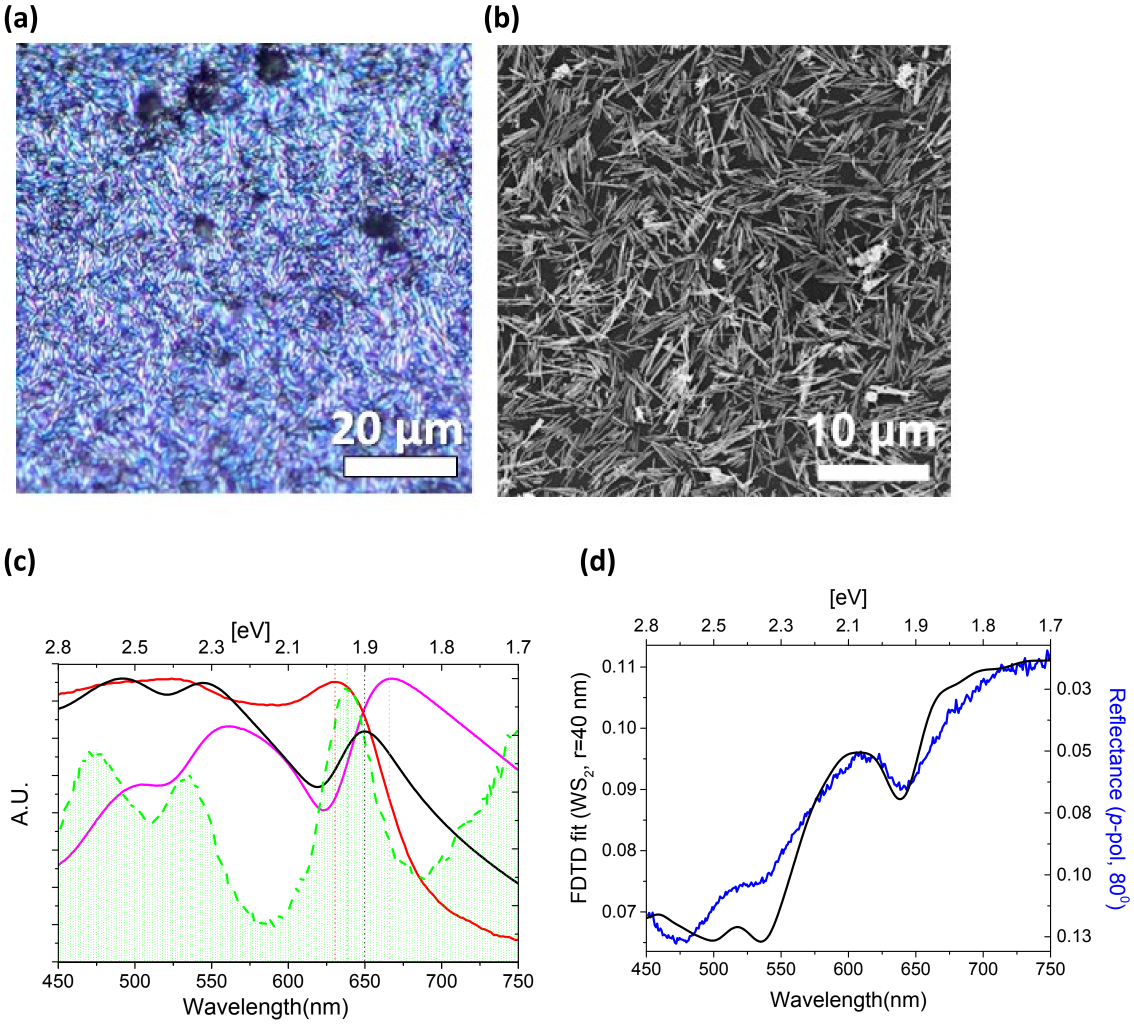

Figure S6. Typical micrograph of WS_2 nanotubes film acquired using **(a)** optical and **(b)** scanning electron microscopy. **(c)** The compression of the reflectance (green) and extinction spectra of this film (black) to the absorbance (red) and extinction (pink) of the dispersed nanotubes. **(d)** Comparison between the reflectance measurements (*p*-pol, θ=80°) and the results of FDTD simulation (WS_2 NT, r=40 nm, perpendicular polarization)

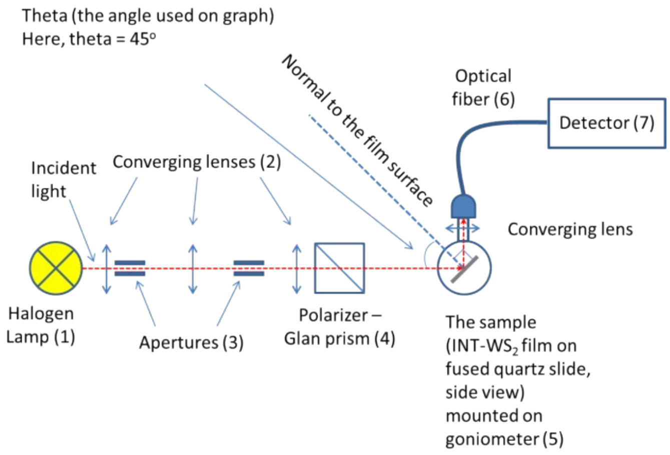

Figure S7. The scheme of the reflectivity measurements set-up. Halogen lamp (1) was used as a light source. The initial light was collimated using converging lenses (2) while apertures (3) were used to shape a parallel light beam (2 mm in diameter). Glan prism (4) mounted on a precisely rotating support was used for controlling the linear polarization of the incident light. The nanotubes WS_2 film was deposited on a fused quartz slide and was mounted on a motorized $\vartheta - 2\vartheta$ goniometer (5). The reflected beam was focused to an optical fiber (6) mounted on a swivel mount of a goniometer and connected to Solar S100 spectrometer (7).

7 Plasmon or cavity mode resonance

Plasmonic or cavity modes are two of the most feasible explanation for the nature of the additional resonance found in the extinction spectra of the dispersed WS_2 nanotubes. Remarkably, there are previous works that in favor of either of these possibilities. However, as the exciton and the extra resonances are intrinsically, as synthesized, coupled. It is impossible to separate this two in order to study each of them separately.

7.1 In favor of plasmonic resonance:

The synthesis of the WS_2 nanotubes is carried out under high-temperature conditions (ca. 800-950 °C) [9] and thus might induce some intrinsic defects and sulfur vacancies in the layers. This is supported by recent studies, which revealed that new energy states within the MS_2 (M=W, Mo) bandgap are induced by the intrinsic defects in the layers.[10] Some of the defects in the nanotubes arise due to the behavior typical of polytypes mixture. While the 2H polytype is the stable form in ambient conditions, the WS_2 nanotubes incorporate defects associated with “patches” of other polytypes, i.e. 1T-like (metallic) and 3R-like [ii] (semiconducting).[10-11] These dislocations, defects and metal “patches”[12] in the lattice can induce an excess of charge carriers on the nanotubes surface.[13] Indeed, a free carrier density of the order of 10^{19} cm^{-3} (corresponds to the plasmonic resonance at 1500 nm) was recently reported for unintentionally doped WS_2 nanotubes.[12] Moreover, the MoS_2 nanoparticles, which belongs to the same family of materials and synthesized in similar conditions with WS_2 NT, have recently been shown to exhibit a plasmonic scattering peak in the near-infrared region.[8c] Remarkably, in addition to the plasmonic scattering, the MoS_2 nanoparticles also retain some of the excitonic structure of the undoped material.[8c] Those findings make WS_2 nanotubes an intriguing material to study also in the plasmonic context.

[ii] Note that the integers here (1, 2, 3) indicate the number of layers per unit cell and T, H, R indicate the trigonal, hexagonal, and rhombohedral primitive unit cells, respectively

8 References

[1] a) R. Coehoorn, C. Haas, R. De Groot, *Phys. Rev. B* 1987, 35, 6203; b) T. Böker, R. Severin, A. Müller, C. Janowitz, R. Manzke, D. Voß, P. Krüger, A. Mazur, J. Pollmann, *Phys. Rev. B* 2001, 64, 235305 (11).

[2] Q. C. Sun, L. Yadgarov, R. Rosentsveig, G. Seifert, R. Tenne, J. L. Musfeldt, *ACS nano* 2013, 7, 3506.

[3] P. A. Lee, *Optical and electrical properties*, D. Reidel publishing company Dordrecht / Boston 1976.

[4] J. I. Pankove, *Optical processes in semi-conductors*, DoverPublications. Inc, 1971.

[5] X. Wu, S. K. Gray, M. Pelton, *Opt. Express* 2010, 18, 23633.

[6] Q. Wang, L. Sun, B. Zhang, C. Chen, X. Shen, W. Lu, *Opt. Express* 2016, 24, 7151.

[7] Y. Li, A. Chernikov, X. Zhang, A. Rigosi, H. M. Hill, A. M. van der Zande, D. A. Chenet, E.-M. Shih, J. Hone, T. F. Heinz, *Phys. Rev. B* 2014, 90, 205422.

[8] a) M. J. Luther, K. P. Jain, T. Ewers, A. P. Alivisatos, *Nat. Mater.* 2011, 10, 361; b) J. A. Faucheaux, A. L. Stanton, P. K. Jain, *J. Phys. Chem. Lett.* 2014; c) L. Yadgarov, C. L. Choi, A. Sedova, A. Cohen, R. Rosentsveig, O. Bar-Elli, D. Oron, H. Dai, R. Tenne, *ACS nano* 2014, 8, 3575.

[9] a) A. Zak, L. S. Ecker, R. Efrati, L. Drangai, N. Fleischer, R. Tenne, *Sens. Transducers J.* 2011, 12, 1; b) A. Zak, L. Sallacan-Ecker, A. Margolin, M. Genut, R. Tenne, *Nano: Brief Rep. Rev.* 2009, 4, 91.

[10] a) A. N. Enyashin, M. Bar-Sadan, L. Houben, G. Seifert, *J. Phys. Chem. C* 2013, 117, 10842; b) A. N. Enyashin, L. Yadgarov, L. Houben, I. Popov, M. Weidenbach, R. Tenne, M. Bar-Sadan, G. Seifert, *J. Phys. Chem. C* 2011, 115, 24586.

[11] L. Houben, A. Enyashin, Y. Feldman, R. Rosentsveig, D. Stroppa, M. Bar-Sadan, *J. Phys. Chem. C* 2012, 116, 24350.

[12] R. Levi, O. Bitton, G. Leitus, R. Tenne, E. Joselevich, *Nano Lett.* 2013, 13, 3736.

[13] a) R. Levi, *Ph.D* Weizmann Institute of Science, Israel, 2015; b) R. Levi, J. Garel, D. Teich, G. Seifert, R. Tenne, E. Joselevich, *ACS nano* 2015, 9, 12224.